

Uncertainty Estimates for Optical Flow with Multi-Hypotheses Networks

Eddy Ilg*, Özgün Çiçek*, Silvio Galesso*, Aaron Klein, Osama Makansi, Frank Hutter, Thomas Brox
University of Freiburg, Germany

{ilg,cicek,galesso,kleinaa,makansio,fh,brox}@cs.uni-freiburg.de

Abstract

Recent work has shown that optical flow estimation can be formulated as an end-to-end supervised learning problem, which yields estimates with a superior accuracy-runtime tradeoff compared to alternative methodology. In this paper, we make the network estimate its local uncertainty about the correctness of its prediction, which is vital information when building decisions on top of the estimated optical flow. For the first time we compare several strategies and techniques to estimate uncertainty in a large-scale computer vision task like optical flow estimation. Moreover, we introduce a new network architecture that enforces complementary hypotheses and provides uncertainty estimates efficiently within a single forward pass without the need for sampling or ensembles. We demonstrate high-quality uncertainty estimates that clearly improve over previous confidence measures on optical flow and allow for interactive frame rates.

1. Introduction

The past research in computer vision has shown that deep networks typically outperform handcrafted approaches in terms of accuracy and speed. Optical flow estimation, as one example, can be formulated as a feed-forward convolutional network (FlowNet) [6, 11]. FlowNet yields high accuracy flow at interactive frame rates, which is relevant for many applications in the automotive domain or for activity understanding. A valid critique of such a learning-based approach is its black-box nature: since all parts of the motion estimation are learned from data, there is no strict understanding on how the problem is solved by the network. Although FlowNet 2.0 [11] was shown to generalize well across various datasets, there is no guarantee that it will also work in different scenarios that contain unknown challenges. In real-world scenarios, such as giving control commands to an autonomously driving car, an erroneous decision can be fatal; thus it is not possible to deploy such a system without information about how reliable the underly-

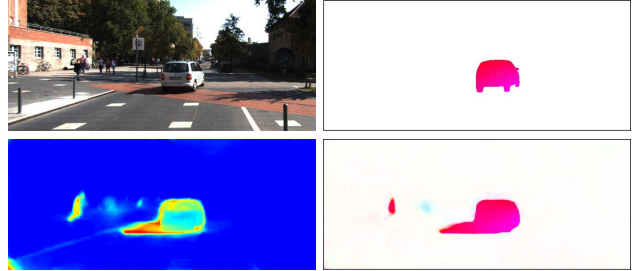


Figure 1: Example from KITTI2015. **Top:** First image and ground-truth flow (pedestrians are excluded from the ground-truth). **Bottom:** Estimated uncertainty (visualized as heatmap) and estimated optical flow. The estimated confidence states that motion estimation in the shadow area is unreliable, contrary to the motion of the car, which is estimated with higher certainty. Most reliable are the estimates for the static background.

ing estimates are. The least one should expect from the network is an estimate of its own uncertainty that would allow the network to highlight hard cases, where it cannot reliably estimate the optical flow or where it must decide upon multiple probable hypotheses; see Figure 1. However, besides few exceptions [14, 24], deep networks in computer vision only yield their single preferred prediction rather than the parameters of a distribution.

The first contribution of this paper is an answer to the open question which of the many approaches for uncertainty estimation, most of which have been applied only to small problems so far, are most efficient for high-resolution encoder-decoder regression networks. We provide a comprehensive study of empirical ensembles, predictive models and predictive ensembles. While the first one is straight-forward and purely empirical, the second one yields the parameters of a distribution, and the third approximates Bayesian neural networks (BNNs). We implemented these approaches for FlowNet using the common MC dropout [7], and the less common Bootstrapped Ensembles [18] and snapshot ensembles [10]. We find that in general all these

*Equal contribution

approaches yield very good uncertainty estimates, where the best performance was achieved with uncertainty estimates derived from Bootstrapped Ensembles of predictive networks.

While such ensembles are a good way to obtain uncertainty estimates, they must run multiple networks to create sufficiently many samples. This drawback increases the computational load and memory footprint at training and test time linearly with the number of samples, such that these approaches are not applicable in real-time.

As a second contribution, we present a multi-headed network architecture that yields multiple hypotheses in a single network without the need of sampling. We use a loss that only penalizes the best hypothesis, which pushes the network to make multiple different predictions in case of doubt. We train a second network to optimally combine the hypotheses and to estimate the final uncertainty. This network yields the same good uncertainty estimates as Bootstrapped Ensembles, but allows for interactive frame rates.

2. Related Work

Confidence measures for optical flow. While there is a large number of optical flow estimation methods, only few of them provide uncertainty estimates. *Post-hoc* methods apply post-processing to already estimated flow fields. Kondermann et al. [15] used a learned linear subspace of typical displacement neighborhoods to test the reliability of a model. In their follow-up work [16], they proposed a hypothesis testing method based on probabilistic motion models learned from ground-truth data. Aodha et al. [20] trained a binary classifier to predict whether the endpoint error of each pixel is bigger or smaller than a certain threshold and used the predicted classifier’s probability as an uncertainty measure. All post-hoc methods ignore information given by the model structure.

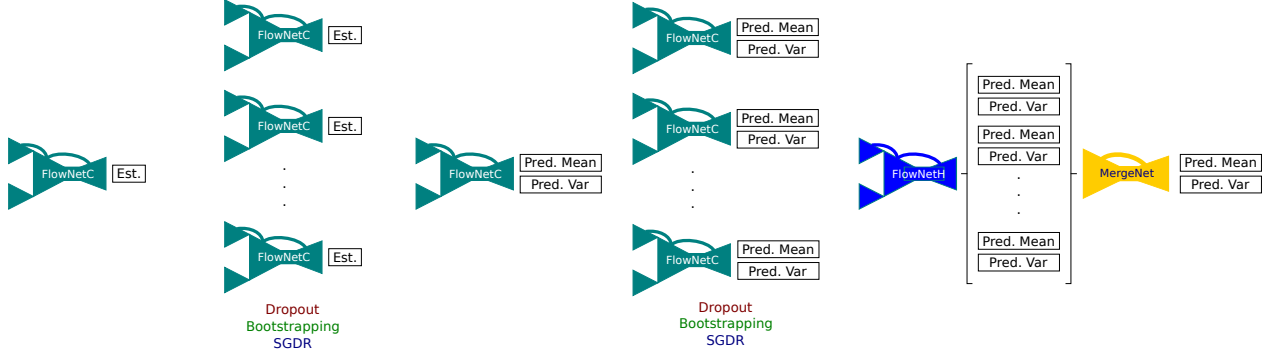
Model-inherent methods, in contrast, produce their uncertainty estimates using the internal estimation model, i.e., energy minimization models. Bruhn and Weickert [3] used the inverse of the energy functional as a measure of the deviation from the model assumptions. Kybic and Nieuwenhuis [17] performed bootstrap sampling on the data term of an energy-based method in order to obtain meaningful statistics of the flow prediction. The most recent work by Wannenwetsch et al. [27] derived a probabilistic approximation of the posterior of the flow field from the energy functional and computed flow mean and covariance via Bayesian optimization. Ummerhofer et al. [26] present a depth estimation CNN that internally uses a predictor for the deviation of the estimated optical flow from the ground-truth. This yields a confidence map for the intermediate optical flow that is used internally within the network. However, this approach treats flow and confidence separately and there was no evaluation for the reliability of the confidence measure.

Uncertainty estimation with CNNs. Bayesian neural networks (BNNs) have been shown to obtain well-calibrated uncertainty estimates while maintaining the properties of standard neural networks [23, 21]. Early work [23] mostly used Markov Chain Monte Carlo (MCMC) methods to sample networks from the distribution of the weights, where some, for instance Hamiltonian Monte Carlo, can make use of the gradient information provided by the back-propagation algorithm. More recent methods generalize traditional gradient based MCMC methods to the stochastic mini-batch setting, where only noisy estimates of the true gradient are available [5, 28]. However, even these recent MCMC methods do not scale well to high-dimensional spaces, and since contemporary encoder-decoder networks like FlowNet have millions of weights, they do not apply in this setting.

Instead of sampling, variational inference methods try to approximate the distribution of the weights by a more tractable distribution [8, 2]. Even though they usually scale much better with the number of datapoints and the number of weights than their MCMC counterparts, they have been applied only to much smaller networks [9, 2] than in the present paper.

Gal and Ghahramani [7] sampled the weights by using dropout after each layer and estimated the *epistemic* uncertainty of neural networks. In a follow-up work by Kendall and Gal [14], this idea was applied to vision tasks, and the *aleatoric* uncertainty (which explains the noise in the observations) and the epistemic uncertainty (which explains model uncertainty) were studied in a joint framework. We show in this paper, that the dropout strategy used in all previous computer vision applications [14, 24] is not the best one, and other strategies yield better results.

In contrast to Bayesian approaches, such as MCMC sampling, bootstrapping is a frequentist method that is easy to implement and scales nicely to high-dimensional spaces, since it only requires point estimates of the weights. The idea is to train M neural networks independently on M different bootstrapped subsets of the training data and to treat them as independent samples from the weight distribution. While bootstrapping does not ensure diversity of the models and in the worst case could lead to M identical models, Lakshminarayanan et al. [18] argued that ensemble model averaging can be seen as dropout averaging. They trained individual networks with random initialization and random data shuffling, where each network predicts a mean and a variance. During test time, they combined the individual model predictions to account for the epistemic uncertainty of the network. We also consider so-called *snapshot ensembles* [10] in our experiments. These are obtained rather efficiently via Stochastic Gradient Descent with warm Restarts (SGDR) [19].



(a) FlowNetC Emp (b) Emp Ensembles (c) FlowNetC Pred (d) Pred Ensembles (e) FlowNetH-Pred-Merged

Figure 2: Overview of the networks and ensembles considered in this paper. **(a)** FlowNetC trained with EPE loss. **(b)** Same network, where an ensemble is built using dropout, bootstrapping or SGDR. **(c)** FlowNetC trained with log-likelihood loss to predict mean and variance. **(d)** Same network, where an ensemble is built using dropout, bootstrapping or SGDR. **(e)** FlowNetH trained to predict multiple hypotheses with variances, which are merged to a single distributional output.

3. Uncertainty Estimation with Deep Networks

In this section we formally describe the concept of uncertainty estimation for CNNs and explain how to apply it to flow estimation. Assume we have a dataset $\mathcal{D} = \{(\mathbf{x}_0, \mathbf{y}_0^{\text{gt}}), \dots, (\mathbf{x}_N, \mathbf{y}_N^{\text{gt}})\}$, which is generated by sampling from a joint distribution $p(\mathbf{x}, \mathbf{y})$. In CNNs, it is assumed that there is a unique mapping from \mathbf{x} to \mathbf{y} by a function $f_{\mathbf{w}}(\mathbf{x})$, which is parametrized by weights \mathbf{w} that are optimized according to a given loss function on \mathcal{D} .

For optical flow, we denote the trained network as a mapping from the input images $\mathbf{x} = (\mathbf{I}_1, \mathbf{I}_2)$ to the output optical flow $\mathbf{y} = (\mathbf{u}, \mathbf{v})$ as $\mathbf{y} = f_{\mathbf{w}}(\mathbf{I}_1, \mathbf{I}_2)$, where \mathbf{u}, \mathbf{v} are the x- and y-components of the optical flow. We base our flow estimation model on the deterministic FlowNet by Dosovitskiy *et al.* [6] and train a variant of FlowNetC on the FlyingChairs dataset to minimize the per-pixel endpoint error:

$$\text{EPE} = \sqrt{(u - u^{\text{gt}})^2 + (v - v^{\text{gt}})^2}, \quad (1)$$

where the pixel location is omitted for brevity. This network, as depicted in Figure 2a, is fully deterministic and yields only the network’s preferred output $\mathbf{y} = f_{\mathbf{w}}(\mathbf{x})$. Depending on the loss function, this typically corresponds to the mean of the distribution $p(\mathbf{y}|\mathbf{x}, \mathcal{D})$. In this paper, we investigate three approaches to model uncertainty. They are based on the empirical mean and variance of the distribution, a parametric model of the distribution, and a combination of both approaches. The variance σ^2 in all these approaches serves as an estimate of the uncertainty.

3.1. Empirical Uncertainty Estimation

A very simple approach to get uncertainty estimates is to train M different models independently, such that the mean and the variance of the distribution $p(\mathbf{y}|\mathbf{x}, \mathcal{D})$ can be

approximated with the empirical mean and variance of the individual model’s predictions. Let $f_{\mathbf{w}_i}(\mathbf{x})$ denote model i of an ensemble of M models with outputs $\mathbf{u}_{\mathbf{w}_i}$ and $\mathbf{v}_{\mathbf{w}_i}$. We can compute the empirical mean and variance for the \mathbf{u} -component by:

$$\mu_{\mathbf{u}} = \frac{1}{M} \sum_{i=1}^M \mathbf{u}_{\mathbf{w}_i}(\mathbf{x}) \quad (2)$$

$$\sigma_{\mathbf{u}}^2 = \frac{1}{M} \sum_{i=1}^M (\mathbf{u}_{\mathbf{w}_i}(\mathbf{x}) - \mu_{\mathbf{u}})^2 \quad (3)$$

and accordingly for the \mathbf{v} -component of the optical flow. Such an ensemble of M networks, as depicted in Figure 2b, can be built in multiple ways. The most common way is via Monte Carlo Dropout [7]. Using dropout also at test time, it is possible to randomly sample from network weights M times to build an ensemble. Alternatively, ensembles of individual networks can be trained with random weight initialization, data shuffling, and bootstrapping as proposed by Lakshminarayanan *et al.* [18]. A more efficient way of building an ensemble is to use M pre-converged snapshots of a single network trained with the SGDR [19] learning scheme, as proposed by Huang *et al.* [10]. We investigate these three ways of building ensembles for flow estimation and refer to them as Dropout, Bootstrapped Ensembles and SGDR Ensembles, respectively.

3.2. Predictive Uncertainty Estimation

Alternatively, we can train a network to output the parameters θ of a parametric model of the distribution $p(\mathbf{y}|\mathbf{x}, \mathcal{D})$. In the literature, Gaussian distributions (where θ parameterizes the distribution’s mean and the variance) are most common, but any type of parametric distribution is

possible. Such networks can be optimized by maximizing their log-likelihood:

$$\log p(\mathcal{D} | \mathbf{w}) = \frac{1}{N} \sum_{i=1}^N \log p(\mathbf{y}_i | \boldsymbol{\theta}(\mathbf{x}_i, \mathbf{w})) \quad (4)$$

w.r.t. \mathbf{w} . The predictive distribution for an input \mathbf{x} is then defined as:

$$p(\mathbf{y} | \mathbf{x}, \mathbf{w}) \equiv p(\mathbf{y} | \boldsymbol{\theta}(\mathbf{x}, \mathbf{w})). \quad (5)$$

Figure 3a shows the distribution over errors of FlowNet on the Sintel clean training dataset [4] when trained using the endpoint error. It reveals that a Laplace distribution fits the underlying error distribution with its long tails better than a Gaussian distribution. Thus, we model the predictive distribution by a Laplacian. The univariate Laplace distribution has two parameters a and b and is defined as:

$$\mathcal{L}(u|a, b) = \frac{1}{2b} e^{-\frac{|u-a|}{b}}. \quad (6)$$

Figure 3b shows that the joint distribution for u and v is axis aligned. This justifies the approximation of the bivariate Laplace distribution by two independent univariate Laplacians for the u and v components of the optical flow vector. The approximation yields:

$$\mathcal{L}(u, v|a_u, a_v, b_u, b_v) \approx \mathcal{L}(u|a_u, b_u) \cdot \mathcal{L}(v|a_v, b_v). \quad (7)$$

We obtain a probabilistic version of FlowNet with outputs a_u, a_v, b_u, b_v by minimizing the negative log-likelihood of Eq. 7 on the dataset \mathcal{D} . As an uncertainty estimate we use the variance of the predictive distribution, which in this case is $\sigma^2 = 2b^2$. This case corresponds to a single FlowNetC predicting flow and uncertainty as illustrated in Figure 2c.

3.3. Bayesian Uncertainty Estimation

From a Bayesian perspective, to obtain an estimate of model uncertainty, rather than choosing a point estimate for \mathbf{w} , we would marginalize over all possible values:

$$p(\mathbf{y} | \mathbf{x}, \mathcal{D}) = \int p(\mathbf{y} | \mathbf{x}, \mathbf{w}) p(\mathbf{w} | \mathcal{D}) d\mathbf{w} \quad (8)$$

$$= \int p(\mathbf{y} | \boldsymbol{\theta}(\mathbf{x}, \mathbf{w})) p(\mathbf{w} | \mathcal{D}) d\mathbf{w}. \quad (9)$$

This integral cannot be computed in closed form, but by sampling M networks $\mathbf{w}_i \sim p(\mathbf{w}|\mathcal{D})$ from the posterior distribution and using a Monte-Carlo approximation, we can approximate its mean and variance as:

$$p(\mathbf{y} | \mathbf{x}, \mathcal{D}) \approx \sum_{i=1}^M p(\mathbf{y} | \boldsymbol{\theta}(\mathbf{x}, \mathbf{w}_i)). \quad (10)$$

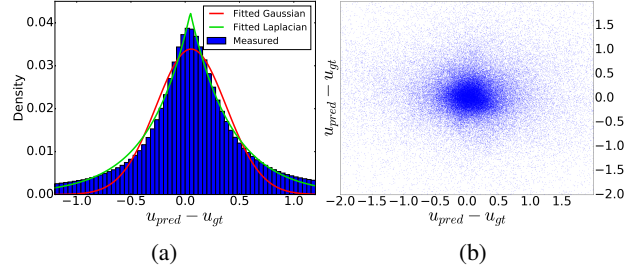


Figure 3: Distribution over errors of the optical flow estimated with FlowNetC on the Sintel train clean dataset. (a) Distribution for the x-component of the error ($u - u^{\text{gt}}$). The error distribution has long tails and is better approximated by a Laplace than by a Gaussian. (b) Scatter plot of the error distribution. The error is axis aligned.

Regardless of which parametric distribution is chosen, the distributions predicted by each individual network with weights \mathbf{w}_i have a mean μ_i and a variance σ_i^2 . The mean and variance of the mixture distribution in Eq. 10 can then be computed by the law of total variance for the \mathbf{u} -component (as well as for the \mathbf{v} component) as:

$$\mu_{\mathbf{u}} = \frac{1}{M} \sum_{i=1}^M \mu_{\mathbf{u},i} \quad (11)$$

$$\sigma_{\mathbf{u}}^2 = \frac{1}{M} \sum_{i=1}^M \left((\mu_{\mathbf{u},i} - \mu_{\mathbf{u}})^2 + \sigma_{\mathbf{u},i}^2 \right). \quad (12)$$

This again can be implemented as ensembles obtained by predictive variants of dropout, bootstrapping or SGDR, where the ideas from Section 3.1 and Section 3.2 are combined as shown in Figure 2d.

4. Predicting Multiple Hypothesis within a Single Network

The methods presented in the Sections 3.1 and 3.3 require multiple forward passes to obtain multiple samples with the drawback of a much increased computational cost at runtime. In this section, we propose a loss function to make multiple predictions within a single network. We call these predictions *hypotheses*. For the predicted hypotheses, we encourage multimodality by the design of the loss function. This makes the predictions more diverse and leads to capturing more different solutions, but does not allow for merging by simply computing the mean as for the ensembles presented in the last section. Therefore, we also propose a second network that merges the hypotheses to a single prediction and variance, as depicted in Figure 2e.

	Sched	EPE
FlowNetC [11]	600k	3.77
FlowNetC [11]	1.2m	3.58
FlowNetC ours	600k	3.40

Table 1: Comparison between the original FlowNetC [11] and implementation in this paper with slightly improved settings on Sintel train clean.

Since ground-truth is available only for the single true solution, the question arises of how to train a network to predict multiple hypotheses and how to ensure that each hypothesis has meaningful information content. Let the loss between a predicted flow vector $\mathbf{y}(i, j)$ and its ground-truth $\mathbf{y}^{\text{gt}}(i, j)$ at pixel i, j be defined by the negative log-likelihood (Section 3.2) and let the predicted hypotheses be denoted as $(\boldsymbol{\mu}_1, \boldsymbol{\sigma}_1), \dots, (\boldsymbol{\mu}_M, \boldsymbol{\sigma}_M)$, consisting of a two-channel mean $\boldsymbol{\mu}_i$ and two-channel variance $\boldsymbol{\sigma}_i$ each. We propose the following loss function:

$$L_{hyp} = \sum_{i,j} l(\boldsymbol{\mu}_{\text{best.idx}(i,j)}(i, j)) + \Delta(i, j), \quad (13)$$

where $\text{best.idx}(i, j)$ selects the best hypothesis per pixel according to the endpoint error of its predicted mean to the ground-truth:

$$\text{best.idx}(i, j) = \underset{k}{\text{argmin}} [\text{EPE}(\boldsymbol{\mu}_k(i, j), \mathbf{y}^{\text{gt}}(i, j))], \quad (14)$$

and $\Delta = \Delta_u + \Delta_v$ enforces similar solutions to lie within the same hypothesis k via one-sided differences, e.g. for the u component:

$$\Delta_u(i, j) = \sum_{k, i>1, j} |\mu_{k,u}(i, j) - \mu_{k,u}(i-1, j)| + \sum_{k, i, j>1} |\mu_{k,u}(i, j) - \mu_{k,u}(i, j-1)| \quad (15)$$

To minimize this loss function, the network must predict the ground-truth in at least one of the hypotheses. In locations where multiple likely solutions exist and the network cannot decide for one of them, the network will predict several different likely solutions to increase the chance that the true solution is among these predictions. Consequently, the network will favor making diverse guesses to increase its chances and the loss triggers dissimilar hypotheses in cases of uncertainty.

5. Experiments

Conventions. When a single network is trained against the endpoint error, we refer to this single network and the resulting ensemble as empirical (abbreviated as *Emp*; Figures

2a and 2b), while when the single network is trained against the negative log-likelihood, we refer to the single network and the ensemble as predictive (*Pred*; Figures 2c and 2d). When multiple samples or solutions are merged with a network, we add *Merged* to the name. E.g. FlowNetH-Pred-Merged refers to a FlowNetH that predicts multiple hypotheses and merges them with a network, using the loss for a predictive distribution for both, hypotheses and merging, respectively (Figure 2e).

5.1. Training Settings

Our networks are based on the FlowNetC architecture from Dosovitsky *et al.* [6] and the settings from Ilg *et al.* [11]. We find that using Batch Normalization [12] and a continuously dropping cosine learning rate schedule [19] yield shorter training times and improve the results (see Table 1). We train on FlyingChairs [6] and start with a learning rate of $2e-4$. For all networks, we fix a training budget of 600k iterations per network, with an exception for SGDR, where we also evaluate performing some pre-cycles. For SGDR Ensembles, we perform restarts every 75k iterations. We fix the T_{mult} to 1, so that each annealing takes the same number of iterations. We experiment with different variants of building ensembles using snapshots at the end of each annealing. We always take the latest M snapshots when building an ensemble. For dropout experiments, we use a dropout ratio of 0.2 as proposed by Kendall *et al.* [14]. For Bootstrapped Ensembles, we train M FlowNetC in parallel with bootstrapping, such that each network sees different 67% of the training data. For the final version of our method, we perform an additional finetuning of 250k iterations on FlyingThings3D [22] per network, starting with a learning rate of $2e-5$ also decaying with cosine annealing. We use the Caffe [13] framework for network training and evaluate all runtimes on an Nvidia GTX 1080Ti.

5.2. Evaluation Metrics and Settings

Sparsification Plots. To assess the quality of the uncertainty measures, we use so-called sparsification plots, which are commonly used for this purpose [20, 27, 16, 17]. Such plots reveal on how much the estimated uncertainty coincides with the true errors. If the estimated variance is a good representation of the model uncertainty, and the pixels with the highest variance are removed gradually, the error should monotonically decrease. Such a plot of our method is shown in Figure 4. The best possible ranking of uncertainties is ranking by the true error to the ground-truth. We refer to this curve as *Oracle Sparsification*. Figure 4 reveals that our uncertainty estimate is very close to this oracle.

Sparsification Error. For each model the oracle is different, hence an evaluation using a single sparsification plot is not possible. To this end, we introduce a new measure, which we name *Sparsification Error*. It is defined as the dif-

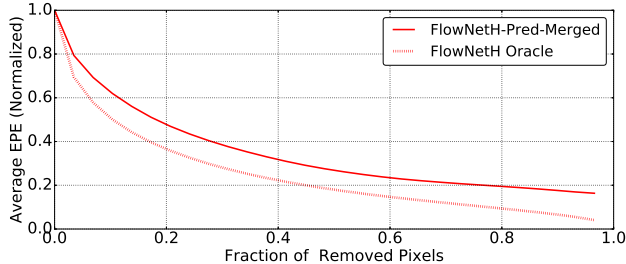


Figure 4: Sparsification plot of FlowNetH-Pred-Merged for the Sintel train clean dataset. The plot shows the average endpoint error (AEPE) for each fraction of pixels having the highest uncertainties removed. The oracle sparsification shows the lower bound by removing each fraction of pixels ranked by the ground-truth endpoint error. Removing 20 percent of the pixels results in halving the average endpoint error.

ference between the sparsification and its oracle. Since this measure is independent of the oracle, a fair comparison of different methods is possible. In Figure 5a, we show sparsification errors for all methods we present in this paper. To quantify the sparsification error with a single number, we use the Area Under the Sparsification Error curve (AUSE).

Oracle EPE. For each ensemble, we also compute the hypothetical endpoint error by considering the pixel-wise best selection from the samples or hypotheses (decided by the ground-truth). We report this error together with the empirical variances among samples and hypotheses in Table 2.

Number of samples. In general, networks for optical flow estimation are large and sampling effort should be minimized. From a set of experiments with FlowNetH, we found that the Oracle EPE monotonically decreases and levels out for $M > 8$. Therefore, we use $M = 8$ as the setting for FlowNetH and as a default setting for the other methods (to limit size and runtime). Figure 5b shows how changing this parameter affects the performance for Dropout, Bootstrapped Ensembles and SGDR Ensembles. For SGDR there is additionally a pre-cycle parameter: snapshots in the beginning have usually not yet converged enough and the number of pre-cycles is the number of snapshots we discard before building the ensemble. In the supplemental material we show that the later the snapshots are taken, the better the results are in terms of EPE. We use 8 pre-cycles in the following experiments.

5.3. Comparison among Uncertainties from CNNs

Figures 5a, 5b and Table 2 show results for all models evaluated in this paper.

Empirical Uncertainty Estimation. From the figures we observe that uncertainty estimation with empirical ensembles is possible, but worse than the other methods pre-

sented in this paper. However, in comparison to predictive counterparts, empirical ensembles tend to yield better EPEs, as will be discussed in the following.

Predictive Uncertainty Estimation. When training against a predictive loss function, the solution is expected to become more robust to outliers, since the network has the possibility to explain these outliers with the uncertainty. This is known as *loss attenuation* [14]. While the EPE loss tries to enforce correct solutions also for outliers, the log-likelihood loss attenuates them. The estimated uncertainty is much better with predictive models than with the empirical ones. Even a single FlowNetC with predictive uncertainty yields much better uncertainty estimates than any empirical ensemble in terms of AUSE. This shows that it is advantageous to let a network estimate its own uncertainty.

Predictive Ensembles. Comparing ensembles of predictive networks to the single network from the last paragraph shows that a single network is actually very close to the predictive ensembles and that the benefit of an ensemble is not large. We attribute this also to loss attenuation: different ensemble members appear to attenuate outliers in a similar manner and induce less diversity, as can be seen by the variance among the members of the ensemble.

When comparing empirical to predictive ensembles we can draw the following conclusions: **a.)** empirical estimation provides more diversity within the ensemble (variance column in Table 2), **b.)** empirical estimation provides lower EPEs and Oracle EPEs, **c.)** all empirical setups provide worse uncertainty estimates than predictive setups.

Ensemble Types. From Figure 5b and Table 2 we see that the commonly used dropout [7, 14] technique performs worst in terms of EPE and AUSE, although the differences between the ensemble types are not very large. SGDR Ensembles provide better uncertainties, yet the variance among the samples is the smallest. This is likely to come from the fact that with SGDR later ensemble members are derived from previous snapshots. Furthermore, because of the 8 pre-cycles, SGDR experiments have the largest number of iterations, which could be an explanation to why they provide the best EPE in comparison to other ensembles. Bootstrapped Ensembles provide the highest sample variance and the lowest AUSE in the predictive case. In conclusion, SGDR could be recommended for empirical and bootstrapping for predictive ensembles.

Ensemble Sizes. Figure 5b shows that in the empirical case, a larger ensemble size in general leads to better uncertainties. Surprisingly, for predictive ensembles it seems that larger ensemble sizes harm uncertainty qualities (with an exception to SGDR). This also motivates the introduction of the proposed merging network investigated in the next paragraph.

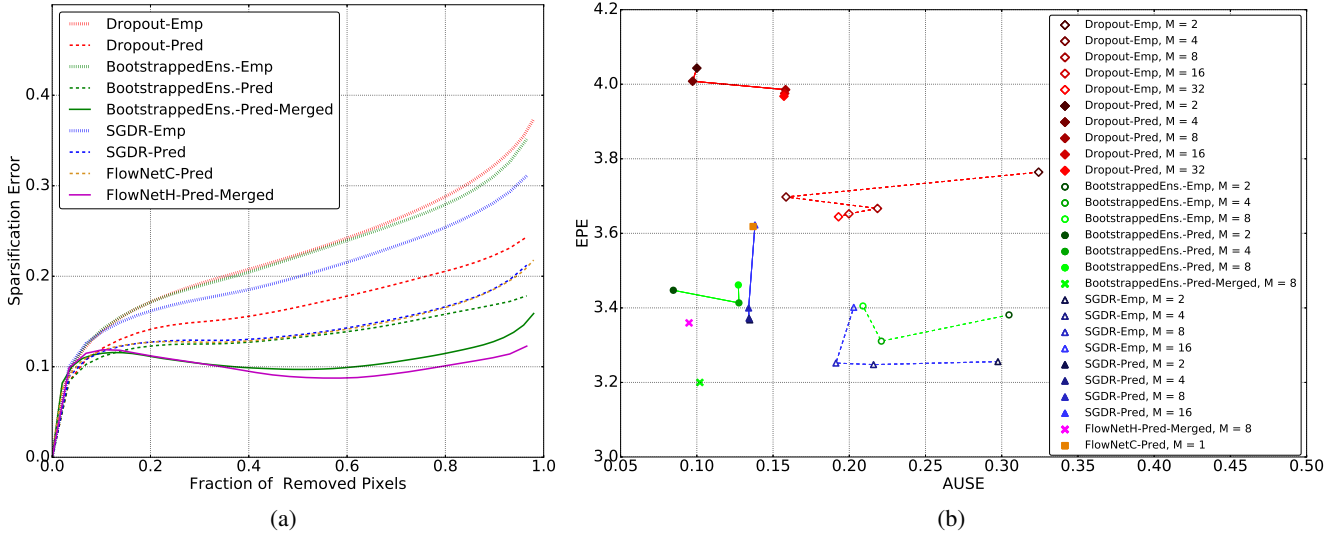


Figure 5: (a) Sparsification error plots on the Sintel train clean dataset. The sparsification error is the proposed measure for evaluating the uncertainty estimations independent of different oracles of different methods. The size of the ensemble is fixed to $M = 8$. FlowNetH-Pred-Merged and BootstrappedEnsemble-Pred-Merged are the best among all. (b) Scatter plot of AEPE vs. AUSE for different proposed ensemble types and sizes.

	empirical (Emp)				predictive (Pred)				Runtime
	EPE	AUSE	Oracle EPE	Var.	EPE	AUSE	Oracle EPE	Var.	
FlowNetC	3.40	-	-	-	3.62	0.133	-	-	38ms
Dropout	3.67	0.212	2.56	5.05	3.99	0.158	2.96	3.80	320ms
SGDREnsemble	3.25	0.191	2.56	3.50	3.40	0.134	2.87	1.52	304ms
BootstrappedEnsemble	3.41	0.209	2.17	9.52	3.46	0.127	2.49	6.15	304ms
BootstrappedEnsemble-Merged					3.20	0.102	2.49	6.15	332ms
FlowNetH-Merged	3.50	-	1.73	83.32	3.36	0.095	1.89	52.85	60ms

Table 2: Comparison of flow and uncertainty predictions of all proposed methods with $M = 8$ on the Sintel train clean dataset. Oracle-EPE is the EPE of the pixel-wise best selection from the samples or hypotheses determined by the ground-truth. Var. is the average empirical variance over the 8 different samples or hypotheses. Predictive versions (Pred) generally outperform empirical versions (Emp) and including a merging network increases performance. FlowNetH-Pred-Merged performs best for predicting uncertainties and has a comparatively low runtime.

Uncertainty Estimation with Merging Networks and FlowNetH. As can be seen from Figure 5b, among the ensembles, the BootstrappedEnsemble-Pred with $M = 2$ is the best in terms of AUSE and the SGDREnsemble-Pred with $M = 2$ is the best in terms of EPE. Introducing FlowNetH-Pred-Merged provides a good trade-off, but is in general not far away from both. However, from Table 2 we see that FlowNetH has a much higher sample variance and the lowest oracle EPE. This indicates that it internally has very diverse and potentially useful hypotheses that could be exploited more in the future. For some visual examples, we refer the reader to Tables 3 and 4 of the supplemental material. For a fair comparison, we also investigate putting a merging network on top of the BootstrappedEnsemble-Pred

with $M = 8$. This provides the best EPE, but in terms of AUSE it is still slightly worse than FlowNetH-Pred-Merged; see Table 2. Although the final results are similar, the base networks consume eight times more memory and runtime. Only FlowNetC and FlowNetH-Pred-Merged allow a deployment at interactive framerates.

5.4. Comparison to Energy-Based Uncertainty Estimation

In this section, we compare our FlowNetH-Pred-Merged to ProbFlow [27], which uses an energy minimization approach and is the currently most accurate method for estimating the uncertainty of optical flow. In Figure 7, we show the sparsification plot together with the sparsification error

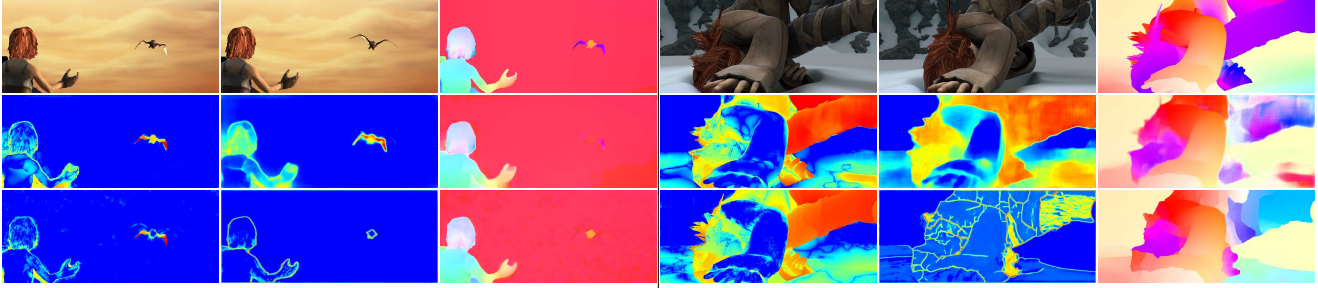


Figure 6: Two examples for qualitative comparison between FlowNetH-Pred-Merged and ProbFlow [27]. The first row shows the image pair followed by its ground-truth flow field for two different scenes from the Sintel clean dataset. The second row shows FlowNetH-Pred-Merged results: entropy from a Laplace distribution with ground-truth error instead of scale parameter (we refer to this as *Oracle Entropy* to represent the optimal uncertainty as explained in the supplemental material), predicted entropy and predicted flow. Similar to the second row, the third row shows the results for ProbFlow. Although both methods fail at estimating the motion of the bird on the left scene and the motion of the leg in the right scene, our method is better at predicting the uncertainties in these regions.

	Sintel		KITTI		runtime
	EPE	AUSE	EPE	AUSE	
ProbFlow [27]	1.87	0.162	8.74	0.554	38.1s [†]
FlowNetH	2.69	0.096	8.35	0.110	60ms
FlowNetH-ft	-	-	3.73	0.099	60ms

Table 3: Comparison to the state-of-the-art method for flow uncertainties: ProbFlow [27] and our FlowNetH-Pred-Merged. We evaluate on the Sintel train clean dataset and our KITTI 12+15 validation split. For this table, FlowNetH-Pred-Merged was finetuned on the FlyingThings3D [22] dataset for 250k iterations and in the last row also subsequently on our KITTI 12+15 training split. One can observe that our method outperforms ProbFlow in AUSE by a large margin and for KITTI also in EPE. [†]runtime taken from [27].

plot for Sintel. We see that ProbFlow has a better oracle but a high sparsification error, while FlowNetH-Pred-Merged has a worse oracle, but is better at estimating the uncertainty of its underlying model.

This is also confirmed by the results from Table 3, which show that FlowNetH consistently outperforms ProbFlow in terms of AUSE. For the KITTI dataset, both EPE and AUSE are better with FlowNetH. Recent work by Ilg et al. [11] showed that using network stacks can further improve the performance of FlowNet. A similar approach could be used to improve the results of FlowNetH in terms of EPE.

Figure 6 shows a qualitative comparison. More results on challenging real-world data are shown in the supplemental video which can also be found on https://youtu.be/UvGY_A-kcrg.

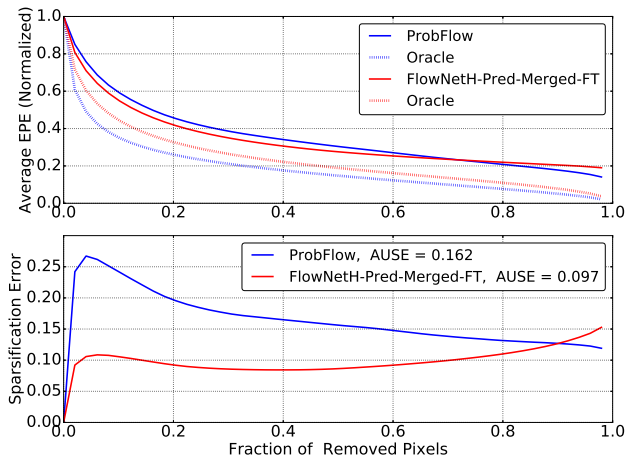


Figure 7: Sparsification (up) and sparsification error (down) plots for ProbFlow and FlowNetH-Pred-Merged-FT on the Sintel clean dataset (FT denotes a version finetuned on FlyingThings3D). KITTI versions are similar and provided in the supplemental material.

6. Conclusion

We presented and evaluated several methods to estimate the uncertainty of deep regression networks for optical flow estimation. We found that SGDR and Bootstrapped Ensembles perform better than the commonly used dropout technique. Furthermore, we found that a single network can estimate its own uncertainty surprisingly well and that this estimate outperforms any empirical ensemble. We believe that these results will apply to many other computer vision tasks, too. Moreover, we presented a multi-hypotheses network that shows very good performance and is faster than sampling-based approaches and ensembles. The fact that

networks can estimate their own uncertainty reliably and in real-time is of high practical relevance. Humans tend to trust an engineered method much more than a trained network, of which nobody knows exactly how it solves the task. However, if networks say when they are confident and when they are not, we can trust them a bit more than we do today.

Acknowledgements

We gratefully acknowledge funding by the German Research Foundation (SPP 1527 grants BR 3815/8-1 and HU 1900/3-1, CRC-1140 KIDGEM Z02) and by the Horizon 2020 program of the EU via the ERC Starting Grant 716721 and the project Trimbot2020.

References

- [1] C. Bailer, B. Taetz, and D. Stricker. Flow fields: Dense correspondence fields for highly accurate large displacement optical flow estimation. In *IEEE Int. Conference on Computer Vision (ICCV)*, 2015. [3](#)
- [2] C. Blundell, J. Cornebise, K. Kavukcuoglu, and D. Wierstra. Weight uncertainty in neural network. In *Proceedings of the 32nd International Conference on Machine Learning (ICML'15)*, pages 1613–1622. [2](#)
- [3] A. Bruhn and J. Weickert. *A Confidence Measure for Variational Optic flow Methods*, pages 283–298. Springer Netherlands, Dordrecht, 2006. [2](#), [1](#)
- [4] D. J. Butler, J. Wulff, G. B. Stanley, and M. J. Black. A naturalistic open source movie for optical flow evaluation. In *European Conference on Computer Vision (ECCV)*, 2012. [4](#), [1](#)
- [5] T. Chen, E. Fox, and C. Guestrin. Stochastic gradient Hamiltonian Monte Carlo. In *Proceedings of the 31th International Conference on Machine Learning, (ICML'14)*, 2014. [2](#)
- [6] A. Dosovitskiy, P. Fischer, E. Ilg, P. Häusser, C. Hazırbaş, V. Golkov, P. v.d. Smagt, D. Cremers, and T. Brox. FlowNet: Learning optical flow with convolutional networks. In *IEEE Int. Conference on Computer Vision (ICCV)*, 2015. [1](#), [3](#), [5](#)
- [7] Y. Gal and Z. Ghahramani. Dropout as a bayesian approximation: Representing model uncertainty in deep learning. In *Int. Conference on Machine Learning (ICML)*, 2016. [1](#), [2](#), [3](#), [6](#)
- [8] A. Graves. Practical variational inference for neural networks. In *In Advances in Neural Information Processing Systems (NIPS) 2011*, page 23482356, 2011. [2](#)
- [9] J. Hernández-Lobato and R. Adams. Probabilistic backpropagation for scalable learning of Bayesian neural networks. In *Proceedings of the 32nd International Conference on Machine Learning (ICML'15)*, 2015. [2](#)
- [10] G. Huang, Y. Li, and G. Pleiss. Snapshot ensembles: Train 1, get M for free. In *Int. Conference on Learning Representations (ICLR)*, 2017. [1](#), [2](#), [3](#)
- [11] E. Ilg, N. Mayer, T. Saikia, M. Keuper, A. Dosovitskiy, and T. Brox. FlowNet 2.0: Evolution of optical flow estimation with deep networks. In *IEEE Conference on Computer Vision and Pattern Recognition (CVPR)*, 2017. [1](#), [5](#), [8](#)
- [12] S. Ioffe and C. Szegedy. Batch normalization: Accelerating deep network training by reducing internal covariate shift. In F. Bach and D. Blei, editors, *Proceedings of the 32nd International Conference on Machine Learning*, volume 37 of *Proceedings of Machine Learning Research*, pages 448–456, Lille, France, 07–09 Jul 2015. PMLR. [5](#)
- [13] Y. Jia, E. Shelhamer, J. Donahue, S. Karayev, J. Long, R. Girshick, S. Guadarrama, and T. Darrell. Caffe: Convolutional architecture for fast feature embedding. In *Proc. ACM MM*, pages 675–678, 2014. [5](#)
- [14] A. Kendall and Y. Gal. What Uncertainties Do We Need in Bayesian Deep Learning for Computer Vision? In *Int. Conference on Neural Information Processing Systems (NIPS)*, 2017. [1](#), [2](#), [5](#), [6](#)
- [15] C. Kondermann, D. Kondermann, B. Jähne, C. S. Garbe, C. Schnörr, and B. Jähne. An adaptive confidence measure for optical flows based on linear subspace projections. 2007. [2](#)
- [16] C. Kondermann, R. Mester, and C. Garbe. *A Statistical Confidence Measure for Optical Flows*, pages 290–301. Springer Berlin Heidelberg, Berlin, Heidelberg, 2008. [2](#), [5](#), [1](#)
- [17] J. Kybic and C. Nieuwenhuis. Bootstrap optical flow confidence and uncertainty measure. *Computer Vision and Image Understanding*, 115(10):1449 – 1462, 2011. [2](#), [5](#), [1](#)
- [18] B. Lakshminarayanan, A. Pritzel, and C. Blundell. Simple and scalable predictive uncertainty estimation using deep ensembles. In *NIPS workshop*, 2016. [1](#), [2](#), [3](#)
- [19] I. Loshchilov and F. Hutter. Sgdr: Stochastic gradient descent with warm restarts. In *Int. Conference on Learning Representations (ICLR)*, 2017. [2](#), [3](#), [5](#)
- [20] O. Mac Aodha, A. Humayun, M. Pollefeys, and G. J. Brostow. Learning a confidence measure for optical flow. *IEEE Transactions on Pattern Analysis and Machine Intelligence (To Appear)*, 2012. [2](#), [5](#), [1](#)
- [21] D. J. C. MacKay. A practical bayesian framework for back-propagation networks. *Neural Computation*, 4(3):448–472, May 1992. [2](#)
- [22] N. Mayer, E. Ilg, P. Häusser, P. Fischer, D. Cremers, A. Dosovitskiy, and T. Brox. A large dataset to train convolutional networks for disparity, optical flow, and scene flow estimation. In *2016 IEEE Conference on Computer Vision and Pattern Recognition (CVPR)*, pages 4040–4048, June 2016. [5](#), [8](#)
- [23] R. Neal. Bayesian learning for neural networks. *PhD thesis, University of Toronto*, 1996. [2](#)
- [24] D. Novotny, D. Larlus, and A. Vedaldi. Learning 3D object categories by looking around them, 2017. [1](#), [2](#)
- [25] J. Revaud, P. Weinzaepfel, Z. Harchaoui, and C. Schmid. EpicFlow: Edge-Preserving Interpolation of Correspondences for Optical Flow. In *IEEE Conference on Computer Vision and Pattern Recognition (CVPR)*, 2015. [3](#)
- [26] B. Ummenhofer, H. Zhou, J. Uhrig, N. Mayer, E. Ilg, A. Dosovitskiy, and T. Brox. Demon: Depth and motion network for learning monocular stereo. In *IEEE Conference on Computer Vision and Pattern Recognition (CVPR)*, 2017. [2](#)

- [27] A. S. Wannenwetsch, M. Keuper, and S. Roth. Probflo: Joint optical flow and uncertainty estimation. In *IEEE Int. Conference on Computer Vision (ICCV)*, Oct 2017. [2](#), [5](#), [7](#), [8](#), [1](#), [3](#)
- [28] M. Welling and Y. Teh. Bayesian learning via stochastic gradient Langevin dynamics. In *Proceedings of the 28th International Conference on Machine Learning (ICML'11)*, 2011. [2](#)

Supplementary Material for "Uncertainty Estimates for Optical Flow with Multi-Hypotheses Networks"

1. Video

Please see the supplementary video for qualitative results on a number of diverse real-world video sequences and a comparison to ProbFlow [27]. The video is also available on https://youtu.be/UvGY_A-kcrg.

2. Color Coding

For optical flow visualization we use the color coding of Butler *et al.* [4]. The color coding scheme is illustrated in Figure 1. Hue represents the direction of the displacement vector, while the intensity of the color represents its magnitude. White color corresponds to no motion. Because the range of motions is very different in different image sequences, we scale the flow fields before visualization: independently for each image pair shown in figures, and independently for each video fragment in the supplementary video. Scaling is always the same for all methods being compared.

For uncertainty visualizations we show the predicted entropy, which we compute as:

$$H = \log(2b_x e) + \log(2b_y e), \quad (1)$$

where b_x and b_y are estimated scale parameters from our Laplace distribution model in x and y dimensions and e is Euler’s number. To assess the quality of our uncertainty estimations, we compare our estimated entropies against the limiting cases, where b_x and b_y correspond to exactly the estimation errors $|u_{pred} - u_{gt}|$ and $|v_{pred} - v_{gt}|$. We visualize this as the *Oracle Entropy* in all cases where ground-truth is present. For ProbFlow [27], the underlying distribution is Gaussian and therefore we use the entropy of a Gaussian distribution:

$$H = 0.5 * \log(2e\sigma_x^2\pi) + 0.5 * \log(2e\sigma_y^2\pi), \quad (2)$$

and set σ_x and σ_y to $|u_{pred} - u_{gt}|$ and $|v_{pred} - v_{gt}|$, respectively. To compare to this oracle entropy we normalize to the same range, but when comparing our method to ProbFlow, we allow to normalize to different ranges to show the most interesting aspects of the entropy.

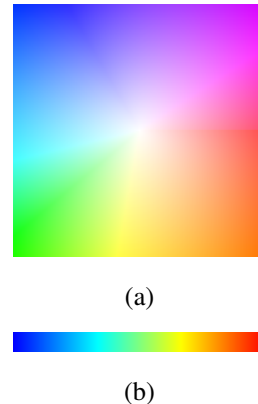


Figure 1: (a) Flow field color coding used in this paper. The displacement of every pixel in this illustration is the vector from the center of the square to this pixel. The central pixel does not move. The value is scaled differently for different images to best visualize the most interesting range. (b) The color coding used for displaying the entropy maps, from the lowest value (blue), to the highest (red).

3. Sparsification Plots

Sparsification is a way to assess the quality of uncertainty estimates for optical flow. Already popular in literature [3, 16, 17, 20], it works by progressively discarding percentages of the pixels the model is most uncertain about and verifying whether this corresponds to a proportional decrease in the remaining endpoint error. To make the results of different experiments comparable, the errors are normalized to 1.

Image-wise sparsification. The method, including the normalization, is typically applied to images individually and the sparsification plots of all images are then averaged. In the main paper we also follow this procedure. However, this approach weights images where the uncertainty estimation is easy equally to images where the uncertainty estimation is hard. Also, due to the normalization, pixels with very large endpoint error from one image can be treated equally to pixels with very small endpoint error from another image.

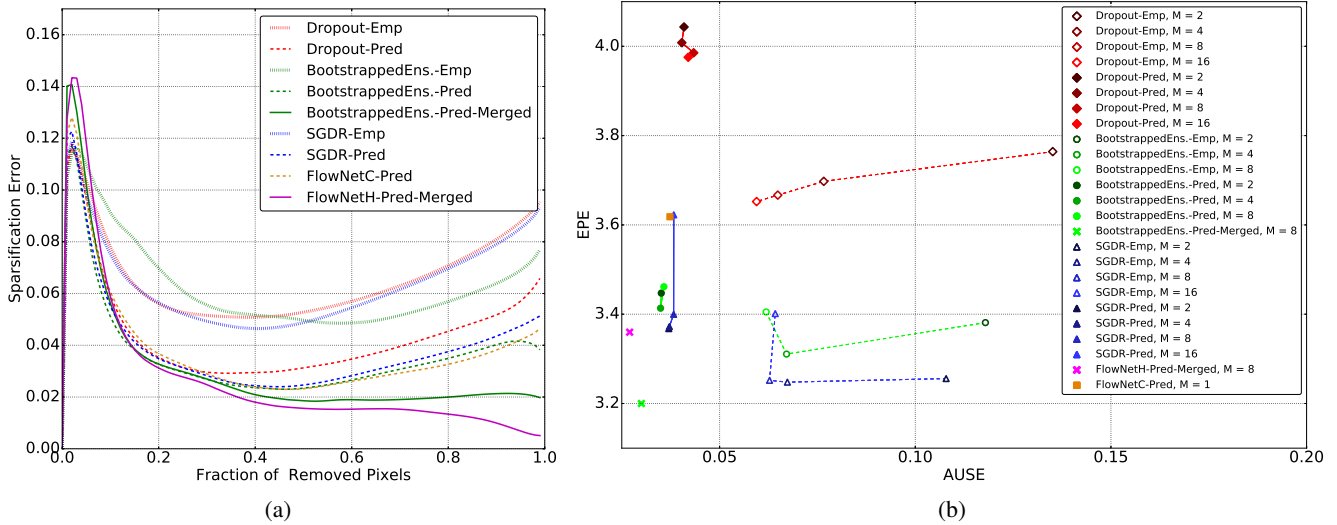


Figure 2: **NOTE: In this version we normalize to the dataset instead of single images.** (a) Sparsification error plots on Sintel train clean dataset. Number of ensemble members are fixed to $M = 8$ and offset for SGDR to 8. We observe that in this case FlowNetH-Pred-Merged and the BootstrappedEnsemble-Pred-Merged perform slightly worse for very high uncertainties, while still showing the best performance for remaining uncertainties. (b) Scatter plot of EPE vs. AUSE for different proposed ensemble types and sizes. For SGDR, we take the last M available snapshots. The behavior of the different models is not drastically different from the one visible in the per-image sparsification scatter plots in Figure 6a from the main paper, with some notable exceptions: the BootstrappedEnsemble-Pred in this case show a more coherent behavior, as do the Dropout-Pred ensembles. The best performing model in terms of AUSE is FlowNetH-Pred-Merged.

Dataset-wise sparsification. Alternatively, one can perform the sparsification on a whole dataset. In this variant, the sparsification is performed first (by ranking across the whole dataset) and normalization is performed last. With this approach, the effect of the outliers is better visible in the sparsification curves, which show larger slopes with respect to the previous method.

In Figures 2a, and 2 we present the figures from the main paper again with the dataset-wise sparsification. In Figure 2a we observe that the BootstrappedEnsemble-Pred-Merged and FlowNetH-Pred-Merged perform slightly worse than other ensembles for very high uncertainties, when sparsified on the whole dataset. However, in Figure 2, the behaviour seems more regular than comparing to Figure 5b from the paper and for most ensembles we see a more linear relationship to the ensemble size. As also observed in the main paper, the AUSE benefit for predictive ensembles is even smaller here.

4. Effect of Offset for SGDR Ensembles

For SGDR ensembles not only the ensemble size M , but also the models discarded from earlier cycles matter (pre-cycles). Therefore, we have further experimented with pre-cycles counts from 0 to 8 (with a constant ensemble size of $M = 8$). The scatter plots of EPE vs. AUSE can be seen in Figure 3. Figure 3a shows the plot where image-wise nor-

malization is used for sparsification, while Figure 3b shows the plot for dataset-wise normalization. From both plots we can see that the later the models are taken, the lower the EPE gets without a significant change in the AUSE measure. When compared to other ensemble types, in SGDR ensembles later models are always derived from earlier models and the later ones are trained for more iterations in total. This might be the reason why they show a lower EPE. However, it also means they can converge more and we actually observe the lowest variance among the models, which can be seen from Table 2 in the main paper.

5. Evaluation on KITTI and Comparison to ProbFlow

We perform the final evaluation of FlowNetH also on the KITTI datasets. We therefore mix KITTI2012 and KITTI2015 and split into 75%/25% training and test data. In Figure 4 and Table 3 from the main paper, we show the performance of our method compared to ProbFlow [27]. As can be seen from Table 3 in the main paper, fine-tuning significantly reduces the endpoint error, as well as AUSE for FlowNetH-Pred-Merged. This concludes that the quality of the uncertainty estimation of FlowNetH-Pred-Merged is outperforming ProbFlow independent of the flow accuracy. For the computation of the KITTI outputs with ProbFlow,

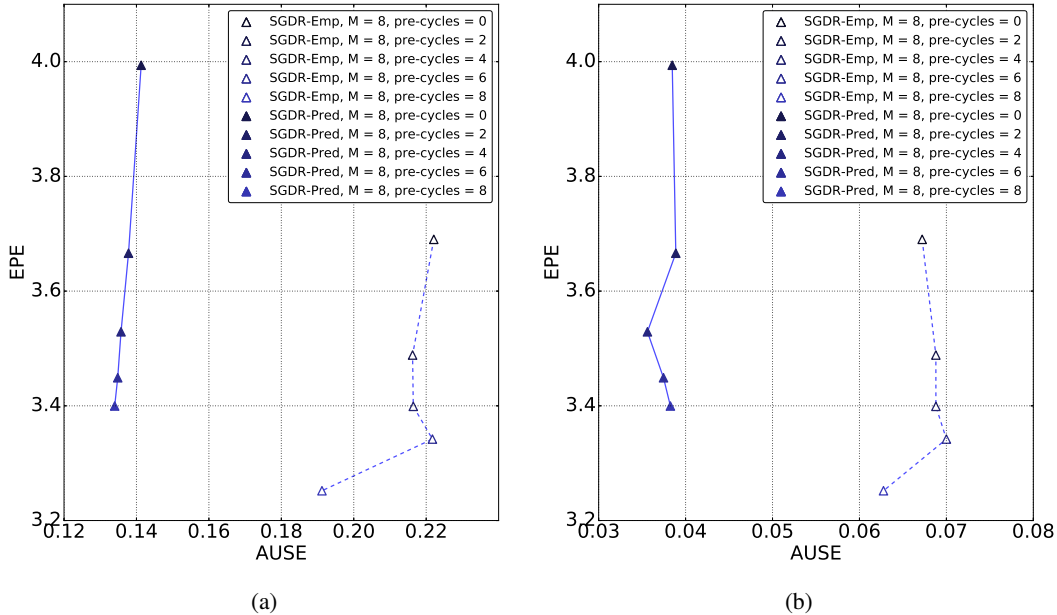


Figure 3: Scatter plot of EPE vs. AUSE showing the effect of different pre-cycle counts for SGDR ensembles with ensemble size $M = 8$. Plot (a) shows the result for the image-wise sparsification. Plot (b) shows dataset-wise sparsification results, both as explained in Section 3. It can be seen that a larger number of pre-cycles always positively affects the EPE without penalizing the AUSE score.

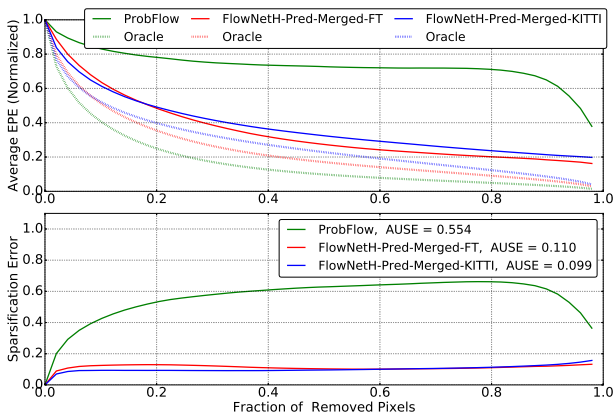


Figure 4: Sparsification and sparsification error plots for ProbFlow [27], FlowNetH-FT (fine-tuned on the FlyingThings3D dataset) and FlowNetH-KITTI (fine-tuned on our joint KITTI2012 and 2015 training dataset). One can observe that fine-tuning does not change the sparsification error, while endpoint errors reduce significantly (see Table 3 of the main paper) and that FlowNetH outperforms ProbFlow. Note that although the average EPE for ProbFlow is higher, due to the effect of normalization the oracle sparsification curve relative to said algorithm appears to be the lowest.

the official software package was used, i.e. flow initializations were obtained from FlowFields [1] matches and interpolated with EpicFlow [25]. For FlowFields we found the best working parameters combination to be $r = 5$, $r_2 = 4$, $\epsilon = 5$, however, the search was conducted around the values suggested in the original paper and a full scale parameter optimization was not performed.

6. Qualitative Evaluation

We provide qualitative results on real world datasets, Sintel train clean, KITTI2012 and KITTI2015 for FlowNetH-Pred-Merged and ProbFlow in Figure 5, Figure 6 and Figure 7.

At last, we show the outputs for all ensemble members for a simple and a difficult case in Tables 1,2 and Tables 3,4. We note that comparing to the other ensembles, hypothesis from FlowNetH generate the most diverse results.

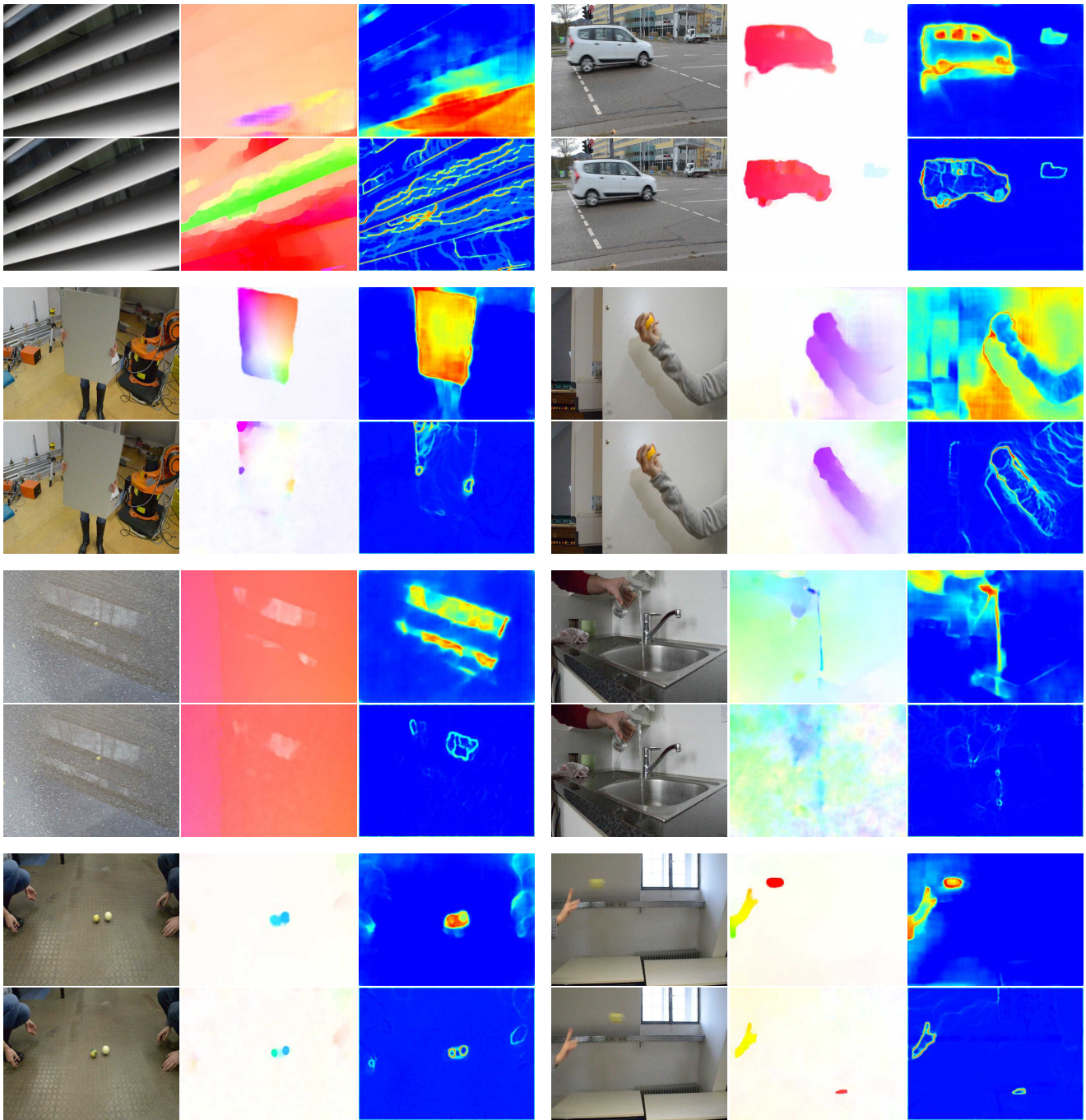


Figure 5: Examples from real world data. Examples are arranged in a coarse 4x2 grid, where in each we follow the convention: **first column:** original image pair, **second column:** flow predicted by FlowNetH-Pred-Merged and flow predicted by ProbFlow, **third column:** predicted entropy by FlowNetH-Pred-Merged and predicted entropy by ProbFlow. **For the full videos of the real world dataset and further comments please see the video on https://youtu.be/UvGY_A-kcrg.**

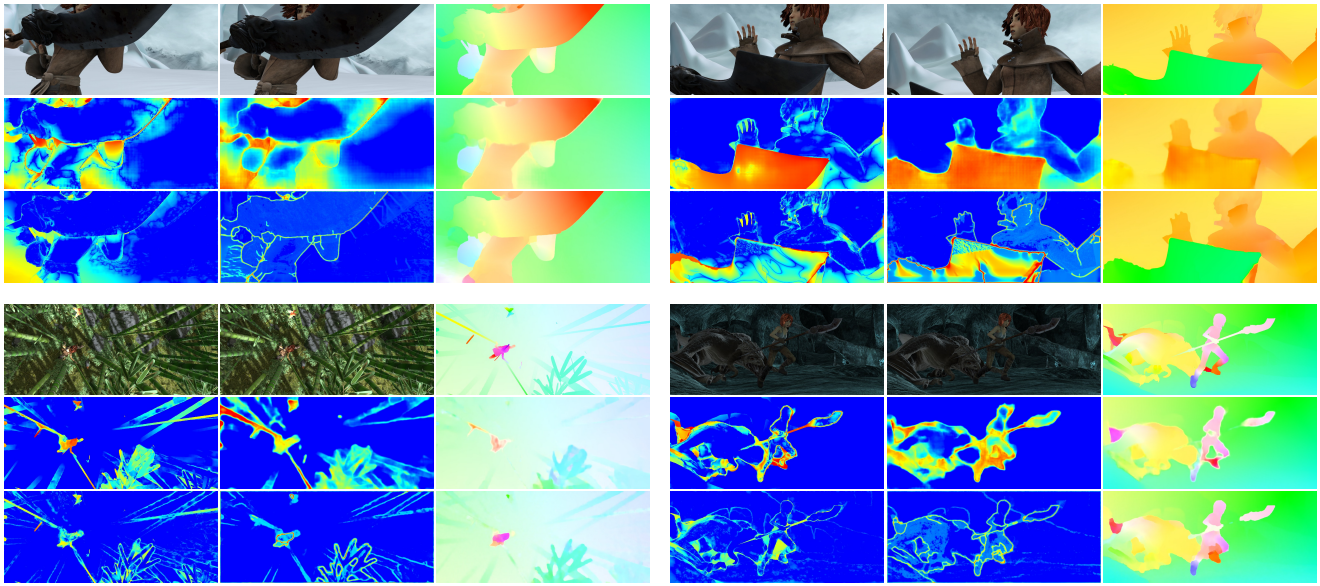


Figure 6: Four examples from the Sintel train clean dataset for qualitative comparison between FlowNetH-Pred-Merged and ProbFlow. For each example: **first row** shows the original image sequence followed by its ground truth flow field. **Second row** shows FlowNetH-Pred-Merged results: oracle entropy (representing the optimal uncertainty), predicted entropy and predicted flow. Similar to the second row, the **third row** shows the results for ProbFlow. While our method is predicting uncertainties on large areas, ProbFlow shows uncertainties mainly only on the motion or image edges and sometimes shows overconfidence in the regions where its prediction is wrong. This is visible e.g. in the lower left example for the upper left corner, where the estimation is wrong, but the uncertainty is low.

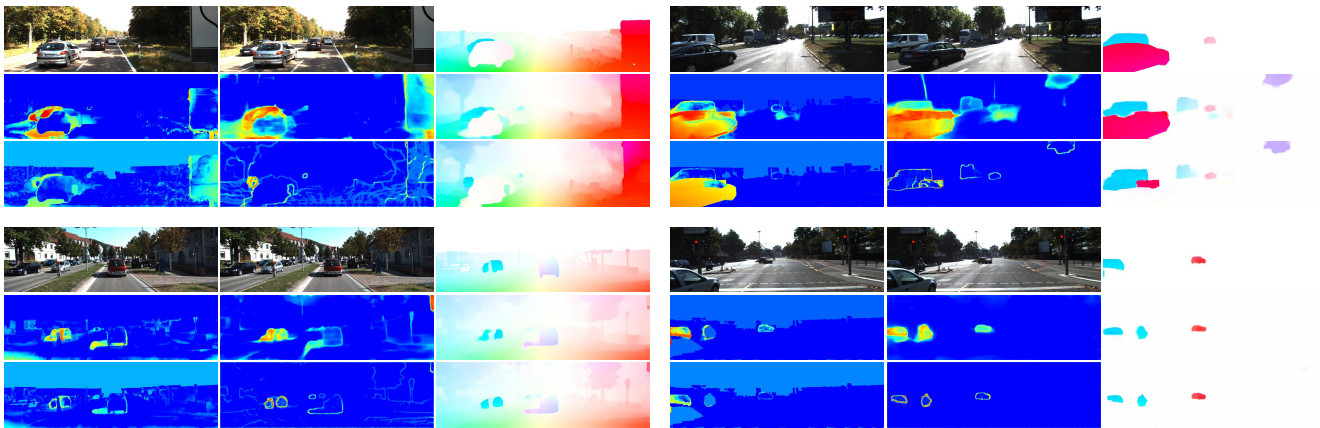


Figure 7: Examples from KITTI2012 and KITTI2015 datasets for qualitative comparison between FlowNetH-Pred-Merged and ProbFlow. For each example: **first row** shows the original image sequence followed by its ground truth flow field (bilinearly interpolated from sparse ground truth). **Second row** shows FlowNetH-Pred-Merged results: oracle entropy (representing the optimal uncertainty), predicted entropy and predicted flow. Similar to second row, **third row** shows the results for ProbFlow. Remark: In the sky the groundtruth provided in the datasets are invalid due to data acquisition.



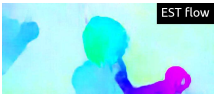
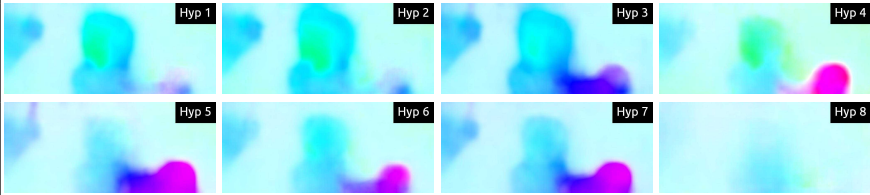
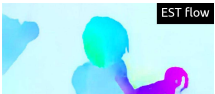
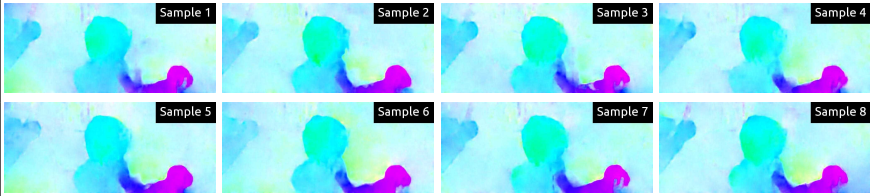
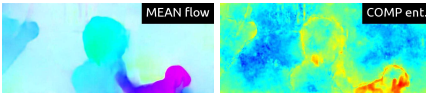
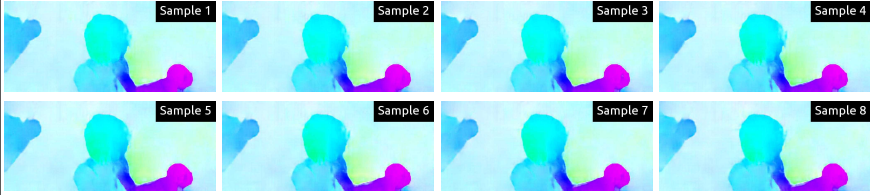
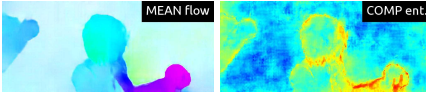
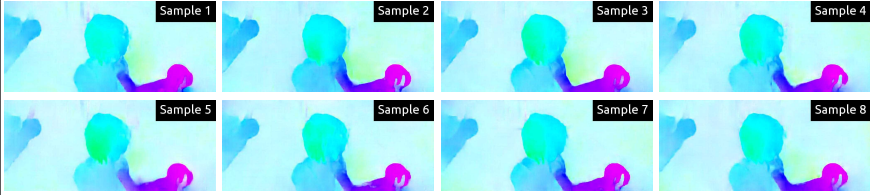
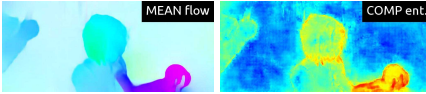
Data: 	
FlowNetC Emp:	
FlowNetH Base: 	
Dropout Emp: 	
SGDR Emp: 	
Bootstrapped Ensemble Emp: 	

Table 1: In this table we show the outputs of empirical experiments with all presented methods for an easy Sintel example as well as the averaged flows and computed entropies. Because the example is easy, the networks are certain and not much variety is visible in the outputs.

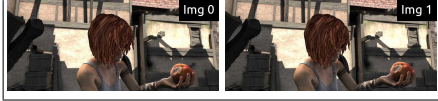

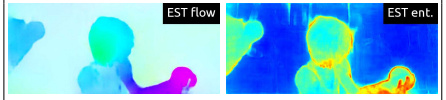
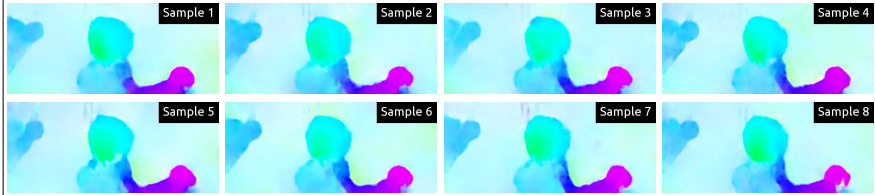
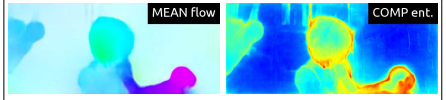
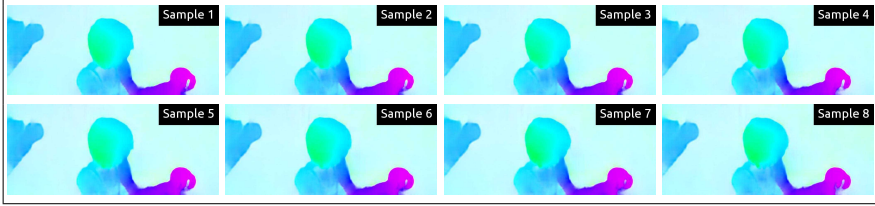
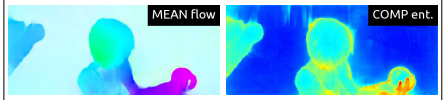
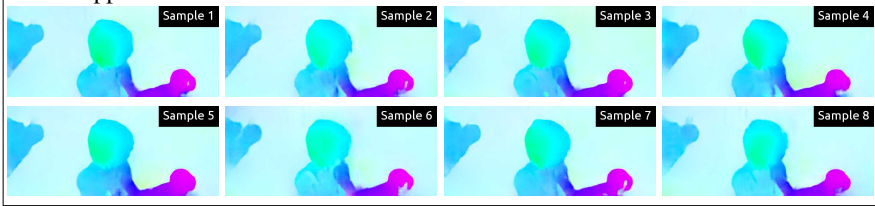
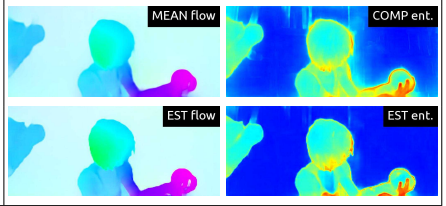
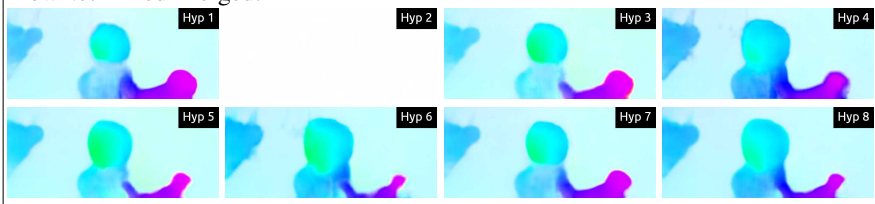
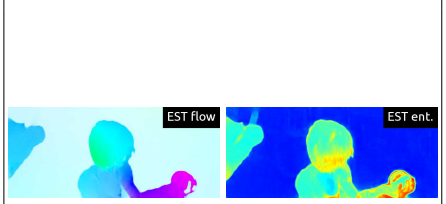
Data: 	 GT flow
FlowNetC Pred:	 EST flow EST ent.
Dropout Pred: 	 MEAN flow COMP ent.
SGDR Pred: 	 MEAN flow COMP ent.
Bootstrapped Ensemble Pred: 	 MEAN flow COMP ent. EST flow EST ent.
FlowNetH Pred-Merged: 	 EST flow EST ent.

Table 2: In this table we show the outputs of predictive experiments with all presented methods for an easy Sintel example as well as the averaged flows and computed entropies. For Bootstrapped Ensemble Pred and FlowNetH Pred Merged we show also the estimated flow and estimated entropy as the output of the merging network on top.



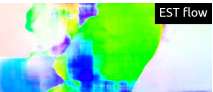
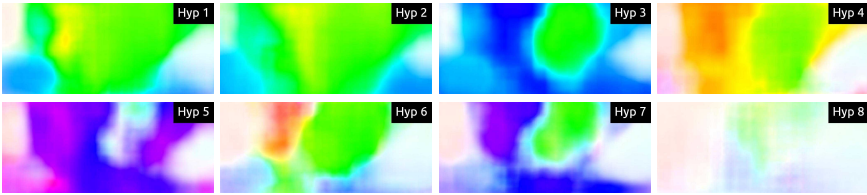

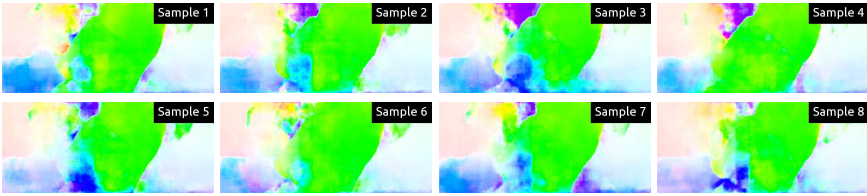
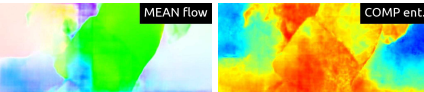
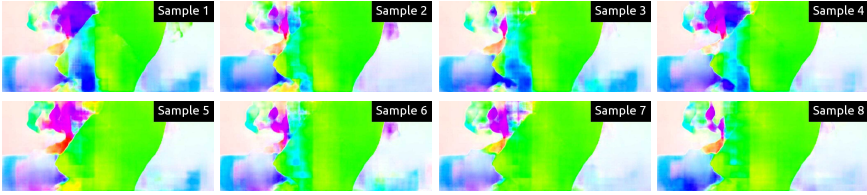
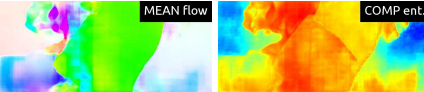
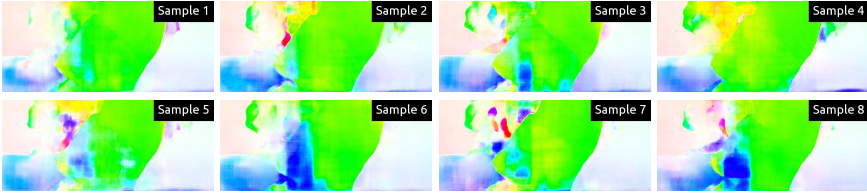
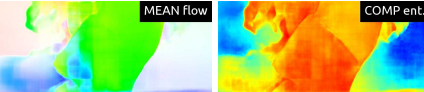
<p>Data:</p> 	
<p>FlowNetC Emp:</p>	
<p>FlowNetH Base:</p> 	
<p>Dropout Emp:</p> 	
<p>SGDR Emp:</p> 	
<p>Bootstrapped Ensemble Emp:</p> 	

Table 3: In this table we show the outputs of empirical experiments with all presented methods for a hard Sintel example as well as the averaged flows and computed entropies. Some variety of each method is visible, while FlowNetH provides a different kind of output with much more variety.

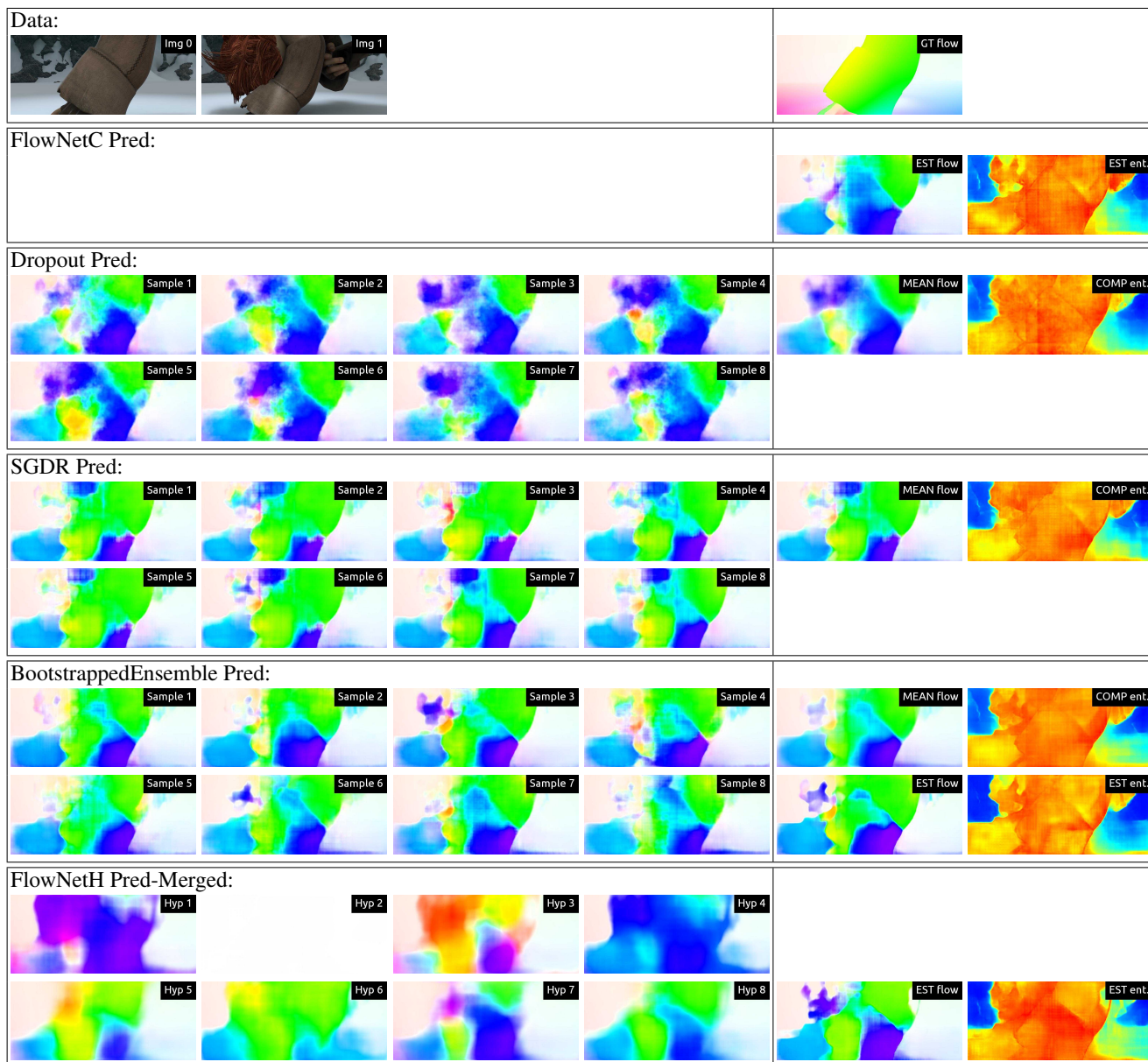


Table 4: In this table we show the outputs of predictive experiments with all presented methods for a hard Sintel example, as well as the averaged flows and computed entropies. For Bootstrapped Ensemble Pred and FlowNetH Pred Merged we show also the estimated flow and estimated entropy as the output of the merging network on top. The hypothesis estimated by FlowNetH Pred Merged is the most diverse one. In the second hypothesis, the motion predicted is very small and could be corresponding to the background.